Net current density of photoelectrons emitted from the surface of the GEOTAIL spacecraft

Tomoko Nakagawa[1], Takuma Ishii[1*], Koichiro Tsuruda[2], Hajime Hayakawa[2], and Toshifumi Mukai[2]

[1]*Tohoku Institute of Technology, 35-1 Yagiyama Kasumi-cho, Taihaku-ku, Sendai, Miyagi 982-8577, Japan*
[2]*The Institute of Space and Astronautical Science, 3-1-1 Yoshinodai, Sagamihara, Kanagawa 229-8510, Japan*

The current density carried by photoelectrons emitted from the GEOTAIL spacecraft is estimated from the electric potential of the spacecraft measured in the single probe mode of GEOTAIL/EFD and plasma density and temperature obtained by GEOTAIL/LEP during the period from September 14, 1993 to October 31, 1998, by assuming balance of the currents carried by photoelectrons and ambient thermal electrons. Behaviour of the photoelectron current as a function of spacecraft potential is consistent with the current profile predicted by Grard (1973), and the emitted photoelectrons consist of several components with different temperatures. The saturation density of the low energy component of the photoelectron current is $85 \pm 33 \times 10^{-6}$ [Am^{-2}]. Number density of the photoelectrons is estimated to be $2.9 \pm 1.4 \times 10^{9}$ [m^{-3}] at the surface of the spacecraft, and the average energy of the photoelectrons is 2.1 ± 0.5 [eV]. These values are higher than the prediction by Grard but consistent with previous in-flight measurements from GEOS-1, ISEE-1 or Viking.

1. Introduction

The electric potential of a sunlit spacecraft in a low-density plasma is strongly affected by emission of photoelectrons from its surface. The spacecraft body is positively charged due to the photoemission current. It comes to an equilibrium potential which is determined by the balance of the currents from escaping photoelectrons and impinging ambient electrons (Mott-Smith and Langmuir, 1926; Fahleson, 1967; Pedersen *et al.*, 1984). Knowledge of the energy distribution of the photoelectrons and the net current carried by them is important for evaluation of measurements of electric field in space.

The density and net current of photoelectrons has been estimated in laboratory experiments and in-situ measurements from spacecraft. Grard (1973) combined laboratory measurements of photoemission from various materials (Feuerbacher and Fitton, 1972) with the best available solar spectrum data collected in space, to determine the density of the photoelectron current in space.

In-flight investigation on the photoelectron current density was carried out from various spacecraft, such as GEOS-1, GEOS-2, and ISEE-1 (e.g., Pedersen *et al.*, 1984; Schmidt and Pedersen, 1987; Pedersen, 1995). In accordance with Langmuir probe theory, the spacecraft potential was a function of electron density, temperature and photoelectron current density (Mozer *et al.*, 1983; Pedersen *et al.*, 1984). Pedersen (1995) suggested that the spacecraft potential can

be used to determine the ambient electron density with limited accuracy but with high time resolution. Escoubet *et al.* (1997) collected measurements of spacecraft potentials from various spacecraft to cover a wide range of plasma density in order to apply them to the ISEE-1 measurement.

The GEOTAIL spacecraft, whose primary purpose was to study the Earth's geomagnetic tail, has an advantage of measuring the spacecraft potential in a wide range of plasma density by the single spacecraft. From measurements of the electric potential, Ishisaka *et al.* (1999) estimated the temperature of ambient electrons in the solar wind and in the electron foreshock region. They treated the energy of photoelectrons as a known parameter. In our study, on the other hand, the energy and the net current of photoelectrons are re-examined by using the spacecraft potential and the ambient plasma parameters, both measured by the GEOTAIL spacecraft over a wide range of plasma parameters.

Section 2 gives a short review of photoemission and electrostatic potentials of surfaces in space. Section 3 describes the data used in this analysis. Section 4 presents the data analysis procedure and the result from GEOTAIL. In Section 5 we will discuss the results and compare them with the prediction by Grard (1973) and with previous measurements in space.

2. Theory of Spacecraft Potential and Photoelectrons

2.1 Balance of currents

The electric potential of a spacecraft in space is determined by the requirement that the net current onto the surface of the spacecraft from the plasma be equal to that flowing from the surface when the input impedance of the voltage measuring circuit is infinite (Mott-Smith and Langmuir, 1926; Fahleson,

---

*Present address: Cable Media Corporation, 3-5-39 Kamisugi, Aoba-ku, Sendai, Miyagi 980-0011, Japan.

1967; Pedersen *et al.*, 1984). The ambient electrons and ions impinging on the surface A of a spacecraft carry the currents

$$I_e = \frac{2}{\sqrt{\pi}} A|q|n_\infty \sqrt{\frac{2k_B T_e}{m_e}} \exp\left(\frac{|q|\phi_{sc}}{k_B T_e}\right) \qquad (1)$$

and

$$I_i = \frac{2}{\sqrt{\pi}} A|q|n_\infty \sqrt{\frac{2k_B T_i}{m_i}}, \qquad (2)$$

respectively, where m_i and m_e are the ion and electron masses, T_i and T_e are their temperatures, k_B is the Boltzmann's constant, n_∞ is the ambient plasma density, and q is the electric unit charge. The photoelectrons emitted from the illuminated surface A_i of the spacecraft carry the current

$$I_{ph} = A_i J(\phi_{sc}) \qquad (3)$$

where ϕ_{sc} is the electric potential of the spacecraft. Secondary electron emission must be considered as an additional process resulting in the current I_{second} flowing into the spacecraft. A floating potential is determined by the balance of these currents. A floating potential is very sensitive to even small variation of these currents. This is undesirable for the probes which should be kept at a stable potential to ensure accurate measurements of ambient electric field. In order to keep the probe potential close to that of the ambient plasma, the bias current, I_{bias}, is driven into the ambient plasma from the probe (Pedersen *et al.*, 1984; Schmidt and Pedersen, 1987). Now the current balance equation is written as

$$-I_e + I_i + I_{ph} + I_{second} - I_{bias} = 0. \qquad (4)$$

In a dense plasma such as in the ionosphere, the currents I_e and I_i from ambient plasmas dominate the photoelectron current I_{ph} and the current of secondary electron emission I_{second}, and hence the spacecraft potential ϕ_{sc} becomes

$$\phi_{sc} = \frac{k_B T_e}{|q|} \log_e \left(\sqrt{\frac{m_e}{m_i}} \sqrt{\frac{T_i}{T_e}} + \frac{I_{bias}}{\frac{2}{\sqrt{\pi}} A|q|n_\infty \sqrt{\frac{2k_B T_e}{m_e}}} \right) \qquad (5)$$

(e.g., Fahleson *et al.*, 1970). In the absence of the bias current I_{bias}, the spacecraft potential becomes negative with respect to that of the ambient plasma and is independent of the density n_∞. When the bias current I_{bias} is large enough, the spacecraft potential becomes approximately proportional to the logarithm of ambient plasma density n_∞.

On the other hand, the photoelectron current I_{ph} becomes important in a low-density plasma, as described in Subsection 2.3.

2.2   Net current carried by photoelectrons

The photoelectron current $I_{ph}(\phi_{sc})$ as a function of spacecraft potential ϕ_{sc} was calculated by Grard (1973).

By combining the energy spectrum $S(\omega)$ of the solar photon energy ω with laboratory measurements of photoelectric yield $Y(\omega)$, i.e., number of electrons emitted per incoming solar photon whose energy is ω, Grard (1973) obtained the total flux of photoelectrons I_s emitted from unit area of a material irradiated by sunlight under normal incidence:

$$I_s = \int_{\omega=0}^\infty Y(\omega)S(\omega)d\omega. \qquad (6)$$

According to Grard (1973), the total flux I_s is 1.9×10^{14} [sec^{-1}m^{-2}] and the saturation current density

$$J_0 = |q|I_s \qquad (7)$$

is 3×10^{-5} [Am^{-2}] for indium oxide, which is the coating material of GEOTAIL.

The flux I_s is the total number of photoelectrons integrated with energy. In order to obtain the net current, we need to know the differential flux of photoelectrons emitted from unit area per unit time as a function of the energy of the photoelectrons, because the low energy components of the photoelectrons emitted from a positively charged spacecraft will return to the body and make no contribution to the net current. Only a fraction of photoelectrons having energies above the spacecraft potential can escape from the surface and contribute to the net current.

The differential flux of photoelectrons emitted per unit time is obtained from the solar spectrum $S(\omega)$, total yield $Y(\omega)$, and energy distribution $f(\omega, \psi)$ of emitted photoelectrons, where $q\psi$ is the energy of the photoelectrons. Grard (1973) introduced a normalized energy spectrum

$$p(\psi) = \frac{1}{I_s} \int_{\omega=0}^\infty Y(\omega)S(\omega)f(\omega, \psi)d\omega \qquad (8)$$

of the photoelectric yield for various materials. Figure 1 shows an example of $p(\psi)$ for indium oxide coating. It should be noted that $p(\psi)$ is not a simple exponential function of ψ, because it reflects complicated profiles of $S(\omega)$, $Y(\omega)$ and $f(\omega, \psi)$.

When a body is assumed to be a point source of photoelectrons, which means that its size is much smaller than the shielding distance for the photoelectrons, we can calculate the net current

$$J(\phi_{sc}) = |q| I_s \int_{\psi=\phi_{sc}}^\infty p(\psi)d\psi \qquad (9)$$

by integrating number of the emitted electrons with energy $|q|\psi$ larger than the surface potential $|q|\phi_{sc}$ of the spacecraft.

When the scale size of a body is much larger than the Debeye length of photoelectrons, direction of the motion of the emitted photoelectrons has to be taken into consideration. In such a case, the net current density is calculated as

$$J(\phi_{sc}) = |q|I_s \int_{\phi=\phi_{sc}}^\infty P(\phi)d\phi \qquad (10)$$

and

$$P(\phi) = \int_{\psi=\phi}^\infty \frac{p(\psi)}{\psi}d\psi, \qquad (11)$$

where $\phi \equiv \frac{1}{2}mv_n^2$ is the photoelectron energy associated with the velocity component v_n normal to the surface of the body (Grard, 1973).

Figure 2 shows the net current density $J(\phi_{sc})$ of photoelectrons from the indium oxide calculated with the point source approximation in the form of Eq. (9) and the plane surface approximation in the form of Eq. (10). Again $J(\phi_{sc})$ cannot be described by a simple function of ϕ_{sc}, however, it will be useful if we find a model function to represent $p(\psi)$ in a limited range of spacecraft potential. Grard (1973) introduced
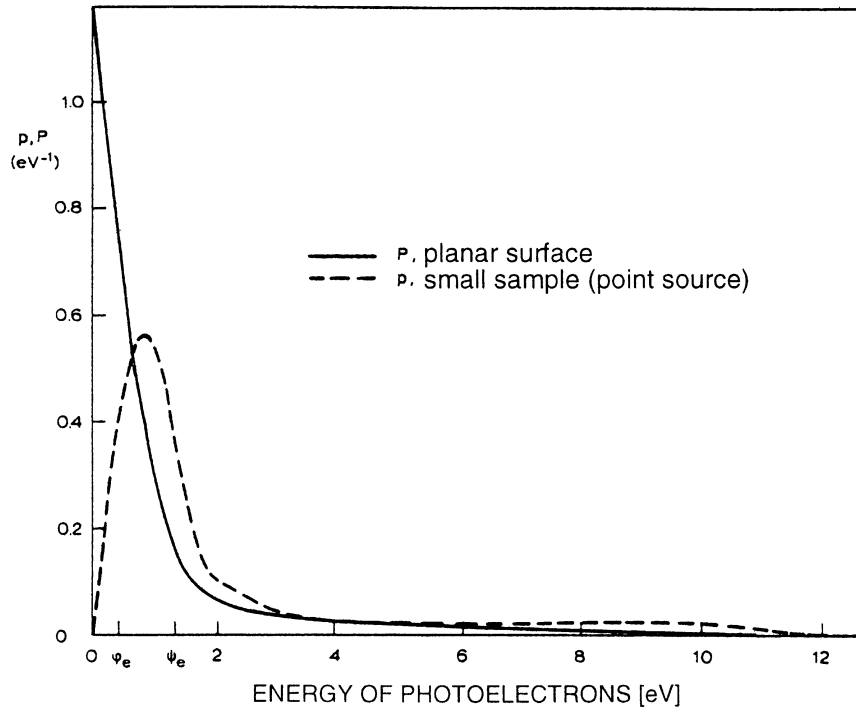
Fig. 1. Normalized photoelectron energy distribution curves of indium oxide under solar irradiation. Energy distribution $P(\phi)$ of electrons emitted from a planar probe is plotted versus the energy ϕ associated with velocity component normal to the surface of the probe (solid line), while the distribution $p(\psi)$ of electrons emitted from a point source is plotted versus the total energy ψ (dashed line). Adapted from Fig. 3(d) of Grard (1973).
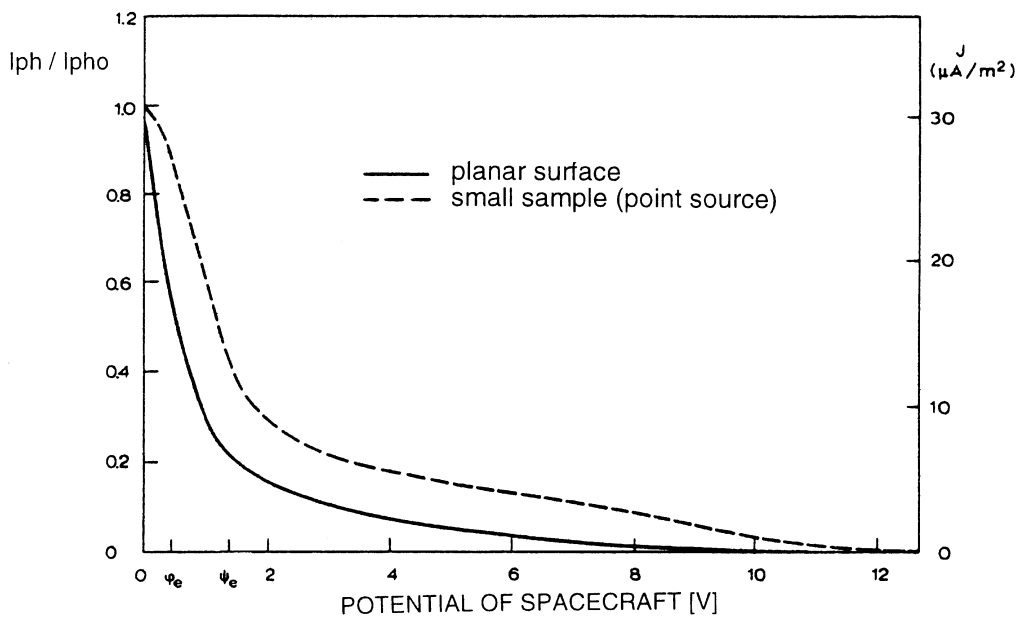

Fig. 2. Normalized photoelectron currents (left-hand scale) or current densities (right-hand scale) of indium oxide under solar irradiation, versus surface potential ϕ_{sc}. The solid line shows the planar probe approximation which corresponds to Eq. (10) and the dashed line shows the point source approximation which corresponds to Eq. (9). Adapted from Fig. 3(e) of Grard (1973).

a model function in the simplest form of

$$p(\psi) \simeq \frac{\psi}{\phi_0^2} \exp\left(\frac{-\psi}{\phi_0}\right), \qquad (12)$$

which leads to an approximation of Eq. (10) which describe the net current density of photoelectrons emitted from large

body

$$J(\phi_{sc}) \simeq J_0 \exp\left(\frac{-\phi_{sc}}{\phi_0}\right) \qquad (13)$$

and an approximation of the photoelectron density N_0 at the

surface of the body

$$N_0 \simeq I_s \sqrt{\frac{2\pi m_e}{|q||\phi_0|}}. \tag{14}$$

According to Grard (1973), the characteristic energy $|q||\phi_0|$ is 1.19 eV and the photoelectron density N_0 is 1.26×10^9 m^{-3} for indium oxide.

Pedersen (1995) and Escoubet *et al.* (1997) tried to approximate the profile of $J(\phi_{sc})$ with a combination of a couple of exponential functions. It should be reminded that they are still approximations.

2.3 Current equilibrium in low-density plasma

In a low-density plasma, the flux of photoelectrons escaping from a sunlit spacecraft becomes as large as that of the flux of ambient electrons impinging onto the spacecraft. The spacecraft potential ϕ_{sc} is automatically adjusted so that I_e and I_{ph}, both functions of ϕ_{sc}, be equal to each other;

$$I_{ph} \simeq I_e, \tag{15}$$

resulting in a positive equilibrium potential of the spacecraft. We can estimate the photoelectron current I_{ph} by calculating I_e from the observations of n_∞ and T_e (Pedersen *et al.*, 1984, Schmidt and Pedersen, 1987). The ion current I_i is negligible with respect to the electron current I_e in a realistic condition where T_i/T_e is less than m_i/m_e. The current I_{second} from secondary electron emissions depends on the ambient electron temperature and is not expected to be important in a region such as the solar wind and the magnetosheath where the energy of incident electrons is low. However it is not the case for the plasmasheet, where the electron temperature is of the order of several hundred eV.

If we employ the simplest approximation of the net photoelectric current of Eq. (13), the current balance is written as

$$A_i J_0 \exp\left(\frac{-\phi_{sc}}{\phi_0}\right) = \frac{2}{\sqrt{\pi}} A|q|n_\infty \sqrt{\frac{2k_B T_e}{m_e}} \exp\left(\frac{|q||\phi_{sc}|}{k_B T_e}\right). \tag{16}$$

It can be easily solved and we obtain the spacecraft potential

$$\phi_{sc} = \frac{\phi_0}{1 + \frac{|q||\phi_0|}{k_B T_e}} \log_e\left(\frac{A_i J_0}{\frac{2}{\sqrt{\pi}} A|q|n_\infty \sqrt{\frac{2k_B T_e}{m_e}}}\right), \tag{17}$$

which is of the order of characteristic energy ϕ_0 of photoelectrons. When the ambient electron energy $k_B T_e$ is much larger than the characteristic energy of photoelectrons $|q||\phi_0|$, the spacecraft potential ϕ_{sc} depends mainly on n_∞ while it has only weak dependence on T_e (Schmidt and Pedersen, 1987).

Current equilibrium on a biased probe with surface area a and sunlit area a_i is written as

$$a_i J_0 \exp\left(\frac{-\phi_{probe}}{\phi_0}\right)$$

$$= \frac{2}{\sqrt{\pi}} a|q|n_\infty \sqrt{\frac{2k_B T_e}{m_e}} \exp\left(\frac{|q||\phi_{probe}|}{k_B T_e}\right) + I_{bias}, \tag{18}$$

when the radius of the probe is larger than the Debeye shielding length for photoelectrons. Here ϕ_{probe} is the potential of the biased probe. Owing to the bias current, the probe potential ϕ_{probe} is made smaller than the floating potential which is of the order of the characteristic energy ϕ_0 of photoelectrons. As ϕ_0 is much smaller than the electron thermal energy in space, we can safely assume that $\frac{|q||\phi_{probe}|}{k_B T_e} \ll 1$ in Eq. (18). It results in the probe potential

$$\phi_{probe} \simeq \frac{\phi_0}{1 + \frac{|q||\phi_0|}{k_B T_e}} \log_e\left(\frac{a_i J_0}{\frac{2}{\sqrt{\pi}} a|q|n_\infty \sqrt{\frac{2k_B T_e}{m_e}} + I_{bias}}\right). \tag{19}$$

When the probe is much smaller than the Debeye length of photoelectrons, the probe potential ϕ_{probe} becomes a little
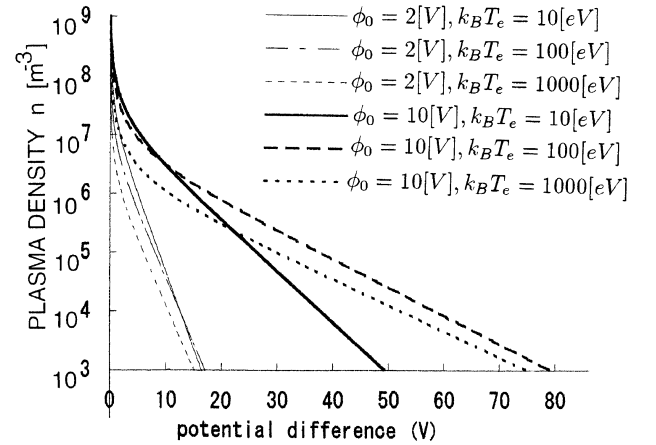
Fig. 3(a). Model calculation of Eq. (20). The ratio $\frac{aA_i}{a_i A}$ is assumed to be 1. Cases for low energy photoelectrons $\phi_0 = 2$ [V] (thin lines) and high energy photoelectrons $\phi_0 = 10$ [V] (thick lines). The thermal energy of ambient electrons $k_B T_e$ is selected to be 10, 100, or 1000 [eV].
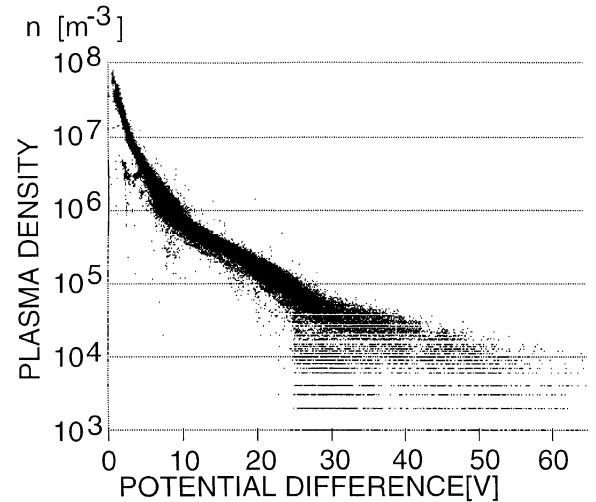
Fig. 3(b). Relationship between the potential difference $\Delta\phi = \phi_{sc} - \phi_{probe}$ measured from GEOTAIL/EFD and ambient plasma density n_∞ measured from GEOTAIL/LEP during the period from November 14, 1993 to December 30, 1993. Data points are plotted every 12 seconds. In spite of probable distribution of plasma temperature, the spacecraft potential is a function of the ambient plasma density. The discrete distribution of the plasma density at $n_\infty \lesssim 3 \times 10^4$ [m^{-3}] is due to rounding errors of the data employed.

larger.

It is useful to derive the potential difference $\Delta\phi = \phi_{sc} - \phi_{probe}$ between the spacecraft and the probe as a function of ambient plasma parameters, because the potential difference $\Delta\phi$, rather than the floating potential ϕ_{sc}, is measured experimentally in space. From Eqs. (17) and (19) we obtain the potential difference

$$\Delta\phi \simeq \frac{\phi_0}{1 + \frac{|q|\phi_0}{k_B T_e}} \log_e \left(\frac{a A_i}{a_i A} \left(1 + \frac{I_{bias}}{\frac{2}{\sqrt{\pi}} a |q| n_\infty \sqrt{\frac{2 k_B T_e}{m_e}}} \right) \right) \tag{20}$$

and the photoelectron current from the illuminated surface A_i of the spacecraft

$$I_{ph}(\Delta\phi) \simeq \frac{A}{a} \frac{I_{bias}}{\frac{a_i A}{a A_i} \exp((\frac{1}{\phi_0} + \frac{|q|}{k_B T_e})\Delta\phi) - 1}. \tag{21}$$

Figure 3(a) shows examples of $n_\infty - \Delta\phi$ curves described by Eq. (20) for several electron temperatures. As the ambient plasma density n_∞ decreases, the potential difference $\Delta\phi$ approaches asymptotically to an exponential function of n_∞.

Figure 3(b) shows the relationship between the ambient plasma density n_∞ and the potential difference $\Delta\phi$ measured from GEOTAIL over a wide range of n_∞. Each point represent a 12-sec observation. In spite of variations in T_e, the data points are concentrated on a curve which is in part described by Eq. (17). The bent in the curve comes from the fact that the photoelectron current I_{ph} cannot be described by a single exponential function of ϕ_{sc}. Similar profiles are found in figure 4 of Schmidt and Pedersen (1987), and figure 8 of Pedersen (1995).

3. Data

The data used in this analysis were obtained from the GEOTAIL spacecraft in the Earth's magnetosphere including the magnetotail, the magnetosheath, and the solar wind, during the period from November 14, 1993 to October 31, 1998. Until November of 1993, the spacecraft had been exposed to solar radiation more than 15 month since its launch on July 24, 1992 (Nishida, 1994).

GEOTAIL has a cylindrical shaped body with diameter of 2.2 [m] and height of 1.6 [m], equipped with a conductive coating of indium oxide (InO_3). As its shape is symmetric around the spin axis which is nearly perpendicular to the sun-spacecraft line, the sunlit area of the spacecraft is approximately constant irrespective of spin phase.

The spacecraft potential is measured every 4 second in SP mode of the electric field detector (EFD) onboard GEOTAIL by using aquadag-coated aluminium sphere probes with diameter of 0.105 [m] (Tsuruda *et al.*, 1994). By applying a proper bias current onto each of the sphere probes mounted at the tips of 50 [m] wires, the potential of the probe is made close to that of the ambient plasma within 1.5–2 [V]. Thus the potential difference $\Delta\phi$ between the spacecraft and the probe gives a measure of the spacecraft potential with respect to the ambient plasma. The optimum magnitude of the bias current of 225 [nA] is determined so that the potential change has minimum sensitivity to the change of the bias current (Tsuruda *et al.*, 1994).

The density and temperature of the ambient plasma are calculated from three-dimensional velocity distributions of ions measured from the energy-per-charge analyzer of the low-energy particle instrument (LEP-EA) every 12 seconds. The energy range of the analyzer is 32[eV/q] to 39[keV/q] for ions and 60 [eV] to 38 [keV] for electrons (Mukai *et al.*, 1994). The electron moment data are not available in the solar wind and in the magnetosheath because the energy range of the electron detector does not cover the core of the thermal electron distributions. In the magnetosphere except for the plasmasheet, photoelectron effects make it difficult to obtain reliable electron moments. Thus in this study, the electron temperature is estimated to be equal to the ion temperature. According to Eq. (1), use of T_i causes overestimation of I_e by 2–3 times in the plasmasheet, where the ratio T_e/T_i is about 1/4–1/7.

Probable uncertainties of the plasma density and temperature are less than 10 per cent in the magnetosphere except for the presence of cold plasma (Matsui *et al.*, 1999). When the plasma density exceeds 7×10^6 [m^{-3}], e.g. in the solar wind, the measurements are affected by saturation of the peak count that causes inaccuracy of the plasma density and the plasma temperature. The plasma data thus obtained are provided in a format in which rounding errors are less than 1 [eV] in temperature and less than 1×10^3 [m^{-3}] or 1×10^4 [m^{-3}] in plasma density received at Usuda Deep Space Center or NASA Deep Space Network, respectively.

4. Photoelectron Current Emitted from GEOTAIL

In order to estimate I_{ph} from Eq. (15) for each ϕ_{sc}, the electron current I_e is calculated from the measurements of plasma parameters and the spacecraft potential by using Eq. (2). The following approximations are made to simplify the calculation:

i) The ion temperature T_i is used in place of the electron temperature T_e,

ii) The temperature is approximated to be isotropic $T_\perp = T_{||}$,

iii) Contribution from energetic particles with anisotropic distribution is ignored,

iv) The shape of the spacecraft is approximated as a simple cylinder with diameter of 2.2 [m] and height of 1.6 [m], which gives the surface $A = 18.7$ [m^2] and the sunlit surface $A_i = 3.5$ [m^2],

v) The probe is considered as a sphere with surface area $a = 3.5 \times 10^{-2}$ [m^2], and any effect from wire was ignored.

Figure 4 shows the photoelectron current I_{ph} calculated from the GEOTAIL observations during the period from September 14, 1993, to December 30, 1993, plotted versus the potential difference $\Delta\phi$ between the spacecraft and the probe. The current profile $I_{ph}(\Delta\phi)$ looks like an exponential function, but it does not decay so fast as an exponential function. It agrees with the curve of $J_{ph}(\phi_{sc})$ in Fig. 2 predicted by Grard (1973) for indium oxide with the planar approximation. The agreement with the planar approximation is better than that with the point source approximation, suggesting that the scale size of the GEOTAIL spacecraft is much larger than the Debeye length of the emitted photoelectrons.

Difference between the current profile $I_{ph}(\Delta\phi)$ and an

Table 1. Photoemissions from GEOTAIL, September 14–December 30, 1993.

range of fitting	$I_{ph}(0)$ [10^{-6} A]	J_0 [10^{-6} Am^{-2}]	ϕ_0 [V]	N_0 [10^6 m^{-3}]	λ_D [m]
GEOTAIL observation, September 14–December 30, 1994					
$1 < \phi_{sc} < 3$	187	53	1.6	1570	0.36
$3 < \phi_{sc} < 6$	72	21	3.0	450	0.91
$6 < \phi_{sc} < 25$	14	4	8.9	50	4.7
Estimation by Grard (1973)					
Indium Oxide		30	1.19	1260	0.20
Aquadag		18	0.83	750	0.24
Viking, calculated by Pedersen (1995) on the basis of Hilgers *et al.* (1992)					
$\phi_{sc} < 7$		48	2		
GEOS-1, calculated by Pedersen (1995)					
$\phi_{sc} < 5$		(50 or 80)	2	500–1000	
ISEE-1, calculated by Pedersen (1995) on the basis of Harvey *et al.* (1978)					
$\phi_{sc} \lesssim 10$		(50 or 80)	2–2.5		

Notes: Results of fitting photoelectron current in the form of $I_{ph}(\phi_{sc}) = I_{ph}(0)\exp(-\frac{\phi_{sc}}{\phi_0})$, or photoelectron current density in the form of $J_{ph}(\phi_{sc}) = J_0 \exp(-\frac{\phi_{sc}}{\phi_0})$, where ϕ_{sc} is spacecraft potential. For GEOTAIL results, $\Delta\phi$ was used in place of ϕ_{sc}. N_0 is photoelectron density at the surface of spacecraft, and λ_D is the Debeye shielding length.
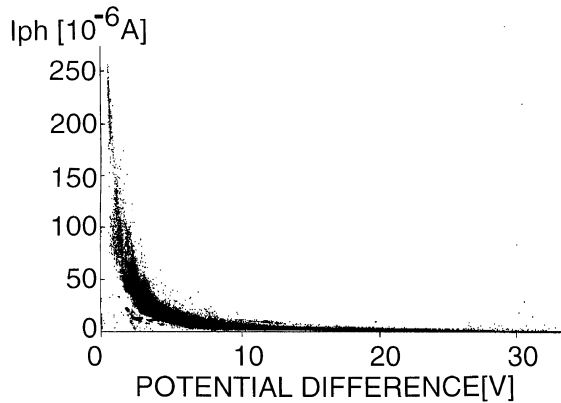

Fig. 4. Photoelectron current I_{ph} calculated from measurements made by GEOTAIL during the period from September 14, 1993 to December 30, 1993, versus the potential difference $\Delta\phi$ between the spacecraft and the probe. The distribution resembles to the current profile for planar probe in Fig. 2.
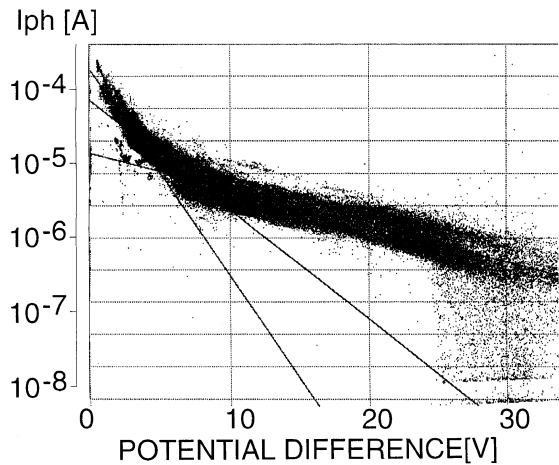

Fig. 5. Logarithm of photoelectron current I_{ph} as a function of potential difference $\Delta\phi \sim \phi_{sc}$. The data set is the same that appeared in Fig. 4. The distribution curve bends at around 3 [V] and 6[V]. Regression lines were drawn for 1–3 [V], 3–6 [V], and 6–25 [V].

exponential function becomes clear when we put the current profile into the logarithmic expression in Fig. 5. The distribution curve bends at $\Delta\phi \simeq 3$ [V] and $\Delta\phi \simeq 6$ [V], indicating that I_{ph} cannot be described by a single exponential function of ϕ_{sc}. Note, however, that it is consistent with Eq. (21) in a limited range $1 \lesssim \Delta\phi \lesssim 3[V]$.

In order to determine model functions for different ranges of $\Delta\phi$, the data set has been divided into 3 parts according to $\Delta\phi$. Table 1 lists the results of fitting a model function in the form of $I_{ph}(\Delta\phi) = I_{ph}(0)\exp(-\frac{\Delta\phi}{\phi_0})$ for each range of $\Delta\phi$, together with the prediction by Grard (1973). The characteristic energy ϕ_0 is estimated to be ~ 1.6 [V] from the regression line of the photoelectron current within the

range $1 < \Delta\phi < 3$ [V]. The average energy $\frac{3}{2}|q|\phi_0$ of the photoelectrons is 2.4 [eV]. Higher characteristic energy ϕ_0 is obtained at higher surface potential ϕ_{sc}.

Estimation of the maximum photoelectron current $I_{ph}(\phi_{sc} = 0)$ is difficult because of the presence of the probe potential ϕ_{probe}. Although ϕ_{sc} differs from $\Delta\phi$ by ϕ_{probe}, it is assumed that ϕ_{probe} is small enough so that $I_{ph}(\phi_{sc})$ can be approximated with $I_{ph}(\Delta\phi)$ in Fig. 5.

From the regression line in the form of $I_{ph}(\Delta\phi) = I_{ph}(0)\exp(-\frac{\Delta\phi}{\phi_0})$, the saturation current is estimated to be $I_{ph}(0) = 187 \times 10^{-6}$ [A] in the range $1 < \Delta\phi < 3$ [V], $I_{ph}(0) = 72 \times 10^{-6}$ [A] in the range $3 < \Delta\phi < 6$ [V], and
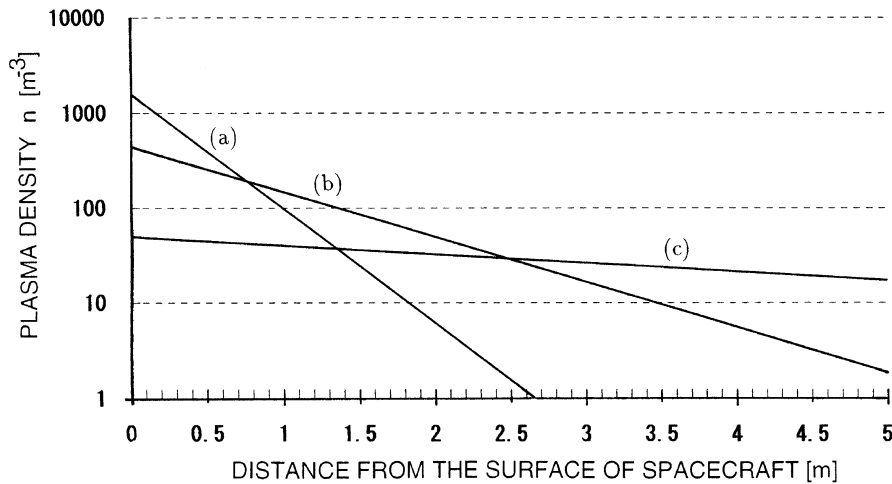
Fig. 6. A model of photoelectron density $N(r) = N_0 \exp(-\frac{r}{\lambda_D})$ as a function of distance r from the surface of the spacecraft. (a) $N_0 = 1570$ [cm^{-3}], $\lambda_D = 0.36$ [m], (b) $N_0 = 450$ [cm^{-3}], $\lambda_D = 0.91$ [m], (c) $N_0 = 50$ [cm^{-3}], $\lambda_D = 4.7$ [m].

$I_{ph}(0) = 14 \times 10^{-6}$ [A] in the range $6 < \Delta\phi < 25$ [V]. Data obtained at $\Delta\phi < 1$ [V] have been excluded from the calculation because the plasma measurement becomes less accurate in high density plasmas, in which the real saturation current is probably by several times $(\exp(\frac{\phi_{probe}}{\phi_0})$ times) larger than it.

Dividing $I_{ph}(0)$ by the sunlit area $A_i \simeq 3.5$ [m^2], we obtain the current density $J_0 = 53 \times 10^{-6}$ [Am^{-2}] under nearly normal light incidence. It is by 77 percent larger than the estimation by Grard (1973). The density of the photoelectrons N_0 near the surface of the spacecraft is 1.57×10^9 [m^{-3}]. The Debeye shielding length $\lambda_D \equiv \sqrt{\frac{3}{2}\frac{\epsilon_0 q \phi_0}{N_0 q^2}}$ of the photoelectrons is 0.36 [m], which is small enough with respect to the dimension of the spacecraft. It is consistent with the fact that the planar surface approximation in Fig. 2, rather than the point source approximation, fits the observed current profile in Fig. 4.

According to Table 1, the best-fit curve of the photoelectron current density $J(\phi_{sc})$ for the data on Fig. 5 is given by

$$J(\phi_{sc}) \, [\mu\text{Am}^{-2}] = 53 \exp\left(-\frac{\phi_{sc}}{1.6}\right) + 21 \exp\left(-\frac{\phi_{sc}}{3.0}\right)$$
$$+ 4 \exp\left(-\frac{\phi_{sc}}{8.9}\right), \qquad (22)$$

where ϕ_{sc} is measured in [V].

It is interesting to see the multi-temperature structure of the emitted photoelectrons. It produces a multi-layered structure of the photoelectron sheath. It is recognized from Table 1 that photoelectrons with a smaller characteristic energy ϕ_0 have larger J_0 and higher concentration N_0 in the vicinity of the spacecraft. Figure 6 illustrates the density of emitted photoelectrons as a function of distance from the surface of the spacecraft. The low-energy component decreases faster than the higher energy component as the distance from the surface increases. At a distance of several meters from the surface, higher energy photoelectrons whose characteristic energy is 8.9 [eV] dominate lower-energy photoelectrons.

The Debeye length λ_D of photoelectrons, which is 0.36 [m] in the vicinity of the spacecraft, becomes up to 4.7 [m], much larger than the diameter of the spacecraft, at a distance of several meters from the spacecraft. The high energy component of the emitted photoelectrons are detected by LEP instrument even when the detector of LEP is in the shade of the spacecraft (not shown here).

5. Discussion
5.1 Comparison with previous studies

The characteristic energy $\phi_0 = 1.6$ [eV] of the photoelectrons as well as the saturation current density $J_0 = 53 \times 10^{-6}$ [Am^{-2}] is larger than those predicted by Grard (1973). It is, however, consistent with previous results from spacecraft observations listed in Table 1. Pedersen (1995) reported that the photoelectron current density was considerably higher in space than in laboratory. Pedersen (1995) calculated ϕ_0 and J_0 from the observations made by GEOS-1, ISEE-1 and Viking, and obtained $\phi_0 = 2$ [V] for GEOS-1, $\phi_0 = 2 \sim 2.5$ [V] for ISEE-1, and $\phi_0 \sim 2$ [V] and $J_0 = 48 \times 10^{-6}$ [A] for Viking. The GEOTAIL results are very close to them.

We cannot exclude another possibility that the simplifications we have made in calculation of I_{ph} caused an overestimation of ϕ_0 and J_0. We have neglected secondary emission of electrons, which is thought to be negligible when the energy of the incident electrons is low (for example, $k_B T_e < 100$ [eV]). It is not the case for the plasmasheet. The plasma sheet data are more likely to be influenced by secondary electron emission as pointed out by Pedersen (1995). He reported that the photoelectron current density was 50–70 percent higher in the plasmasheet than in the solar wind at a spacecraft potential of 9–12 [V], suggesting that the secondary electron emission might influence the result in the plasma sheet.

5.2 Change in slope of photoelectric current profile

The real photoelectric current density $J_{ph}(\phi_{sc})$ cannot be described by a single exponential function in the form of Eq. (13). The current profile bends so that ϕ_0 becomes larger as the spacecraft potential ϕ_{sc} becomes higher. It is consistent
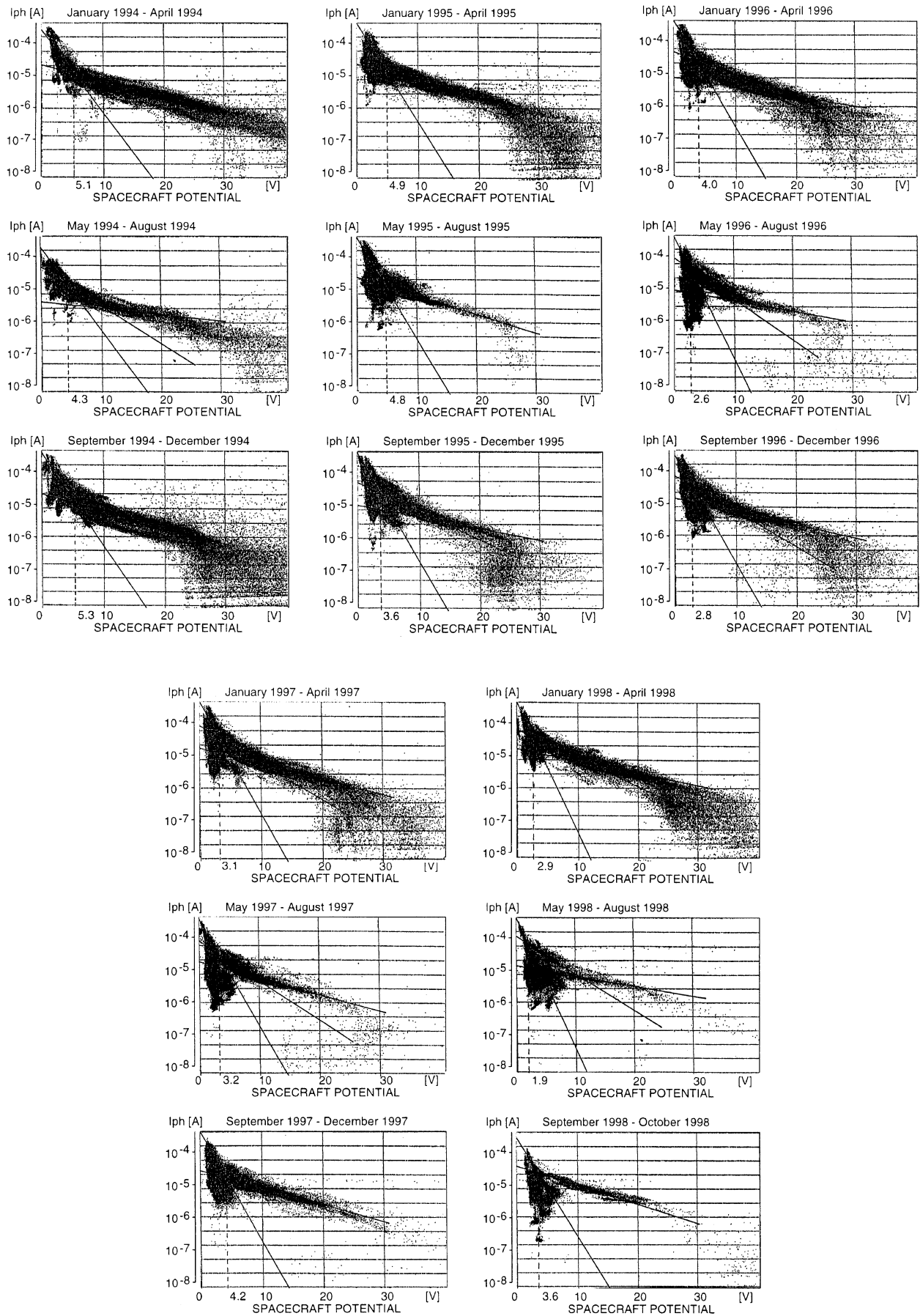
Fig. 7. Photoelectron current I_{ph} calculated from GEOTAIL observation for every 4-month periods starting from January 1, 1994, to October 31, 1994. Dashed lines indicate the spacecraft potential at which the current profile bends.

Table 2. Photoemissions from GEOTAIL, January 1994–October 1998.

Period	fitting range ϕ_{sc} [V]	J_0 [10^{-6} Am^{-2}]	ϕ_0 [V]	N_0 [10^6 m^{-3}]	solar flux* [10^{-22} Wm^{-2}Hz^{-1}]
Sep.–Dec. '93	1–3.0	53	1.6	1570	97.0
Jan.–Apr. '94	1–5.1	72	1.7	2140	96.0
May–Aug. '94	1–4.3	52	1.7	1500	78.5
Sep.–Dec. '94	1–5.3	97	1.5	2920	82.9
Jan.–Apr. '95	1–4.9	119	1.4	3690	82.7
May–Aug. '95	1–4.8	119	1.4	3690	74.7
Sep.–Dec. '95	1–3.6	119	1.3	3890	74.1
Jan.–Apr. '96	1–4.0	119	1.3	3890	71.5
May–Aug. '96	1–2.6	119	1.1	4280	70.6
Sep.–Dec. '96	1–2.8	80	1.3	2530	73.5
Jan.–Apr. '97	1–3.1	119	1.3	3890	74.3
May–Aug. '97	1–3.2	97	1.3	3110	74.1
Sep.–Dec. '97	1–4.2	119	1.3	3890	93.2
Jan.–Apr. '98	1–2.9	119	1.1	4280	100.1
May–Aug. '98	1–1.9	119	1.1	4280	116.4
Sep.–Oct. '98	1–3.6	80	1.4	2530	127.8

*The 10.7 cm Solar Flux from The Solar Radio Monitoring Programme of the National Research Council of Canada (http://www.drao.nrc.ca/icarus/www/intro.html).

with the current profile obtained by Grard (1973), although his calculation was limited within a range of $\phi_{sc} \lesssim 13$ [V]. This is a common feature of the photoelectron current reported from GEOS-1, ISEE-1, and Viking (Pedersen, 1995). It is due to the energy distribution of photoelectric yield $Y(\omega)f(\omega, \psi)$ which becomes flatter and smaller at higher photoelectron energy ψ, and the solar spectrum $S(\omega)$ which becomes weaker at higher photon energy ω (Grard, 1973). When the spacecraft potential ϕ_{sc} is largely positive, only high-energy electrons can contribute to the net current. The number of high-energy photoelectrons is not sensitive to variations of the surface potential ϕ_{sc}. On the other hand, on slightly positive ϕ_{sc}, the number of photoelectrons is very sensitive to even small variations of the spacecraft potential. Indeed, ϕ_0 is calculated from Eq. (13) as

$$\phi_0 \simeq -\frac{1}{\frac{\partial}{\partial \phi_{sc}}(\log_e J(\phi_{sc}))}. \qquad (23)$$

Figure 2 shows that the curve of $J(\phi_{sc})$ is steeply inclined at low ϕ_{sc} for a planar surface, and becomes flatter at higher ϕ_{sc}, which results in small ϕ_0 at low ϕ_{sc} and large ϕ_0 at high ϕ_{sc}.

The change in slope of $I_{ph}(\phi_{sc})$ has been always observed at $\phi_{sc} = 1.9$ [V] ~ 5.3 [V]. Figure 7 shows the $I_{ph} - \phi_{sc}$ distributions produced for every 4 month periods starting from January, 1994, to October, 1998, with regression lines drawn by visual inspection. The bends in the I_{ph} profile are marked with the vertical, dashed lines. Sometimes a second bend is found in the $I_{ph}(\phi_{sc})$ curve at around $\phi_{sc} \sim 10$ [V],

for example, in May–August, 1996, September–December, 1996, and May–August, 1997 of Fig. 7.

5.3 Long-term variation of photoemission

Figure 7 has been produced to see possible long-term variation of the emission of photoelectrons which must be influenced by temporal variation of solar ultraviolet irradiance. A 4-month period is required for each panel to cover a wide range of spacecraft potential. It should be noted that Fig. 7 includes the effect from the change of orbit of GEOTAIL in November 1994 from distant tail trajectories whose apogees were beyond 200 R_E to near-Earth equatorial orbits with apogees ∼30 R_E.

Long-term variation is not clear in Fig. 7 and the overall profile of photoelectron current seems to be rather invariant, although some of the data points deviate from it clustering to form some branches, which appear differently depending on the period.

Table 2 lists the photoelectron currents determined from the regression lines in each panel of Fig. 7 together with the 10.7 cm Solar Flux obtained from the National Research Council of Canada as an indicator of the solar ultraviolet emission. The current density J_0 and the characteristic energy ϕ_0 are in the range of $85 \pm 33 \times 10^{-6}$ [Am^{-2}] and 1.4 ± 0.3 [V], respectively. The average energy of the photoelectrons is 2.1 ± 0.5 [eV], and the number density N_0 at the surface of the spacecraft is within a range of $2.9 \pm 1.4 \times 10^9$ [m^{-3}].

In Table 2, no clear relationship is found between the photoemission and the 10.7 cm Solar Flux, in disagreement with
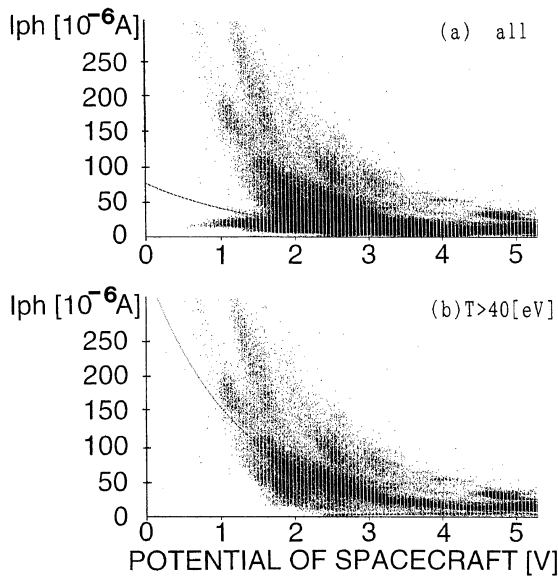
Fig. 8. Photoelectron current distribution with limitation in ambient plasma temperature. The data were obtained during the period from May, 1995 to August, 1995. The regression lines are obtained by method of least squares.

the earlier work by Brace *et al.* (1988). They obtained photoelectron current from the Pioneer Venus Langmuir probe near the Venus, and have found photocurrent variations related to the solar cycle and solar rotation, as well as a major 7.2-month periodicity. The variations well correlated with the temporal variations of the 10.7cm Solar Flux observed at the Earth.

The absence of correlations between our photoelectron current and the 10.7 cm Solar Flux may be due to our selection of duration of the 4-month period. However, since there was the correlation on a longer time scale in Brace *et al.*'s report (1988), it is unlikely that the correlation has been masked by the 4-month average. Perhaps it is mainly due to the difficulty in our fitting procedure. We have drawn the regression lines by visual inspections because the regression lines are very sensitive to the presence or absence of branches in the $I_{ph}(\phi_{sc})$ distribution which deviate from the main profile. Figure 8 shows a difference of the regression lines which are obtained numerically. A branch of $I_{ph}(\phi_{sc}) - \phi_{sc}$ distribution in the lower-left of the panel disappears by limiting plasma temperature. They are mainly from the solar wind. It is likely that the branches in $I_{ph}(\phi_{sc}) - \phi_{sc}$ distribution are caused by variability in the plasma condition which causes difference in accuracy of plasma measurements and quality of the approximations we have made in calculation of I_{ph}.

6. Conclusion

Behaviour of the photoelectron current emitted from the GEOTAIL spacecraft as a function of the spacecraft potential is consistent with the current profile estimated by Grard (1973). The photoelectric current is not described by a single exponential function of the spacecraft potential. The characteristic energy of the photoelectrons is higher at higher space-craft potential. The saturation density of the photoelectron current is $85 \pm 33 \times 10^{-6}$ [Am^{-2}] and the average energy of the photoelectrons is 2.1 ± 0.5 [eV], both higher than Grard's prediction. The number density is $2.9 \pm 1.4 \times 10^9$ [m^{-3}] at the surface of the spacecraft.

References

Brace, L. H., W. R. Hoegy, and R. F. Theis, Solar UV measurements at Venus based on photoelectron emission from the Pioneer Venus Langmuir probe, *J. Geophys. Res.*, **93**, 7282–7296, 1988.

Escoubet, C. P., A. Pedersen, R. Schmidt, and P. A. Lindqvist, Density in the magnetosphere inferred from ISEE 1 spacecraft potential, *J. Geophys. Res.*, **102**, 17595–17609, 1997.

Fahleson, U., Theory of electric field measurements conducted in the magnetosphere with electric probes, *Space Sci. Rev.*, **7**, 238–262, 1967.

Fahleson, U. V., M. C. Kelley, and F. S. Mozer, Investigation of the operation of a d.c. electric field detector, *Planet. Space Sci.*, **18**, 1551–1561, 1970.

Feuerbacher, B. and B. Fitton, Experimental investigation of photoemission from satellite surface materials, *J. Appl. Phys.*, **43**, 1563, 1972.

Grard, R. J. L., Properties of satellite photoelectron sheath derived from photoemission laboratory measurements, *J. Geophys. Res.*, **78**, 2885–2906, 1973.

Harvey, C. C, J. Etcheto, J. De Javel, R. Manning, and M. Petit, ISEE electron density experiment, *IEEE Trans. Geosci. Electron.*, **GE-16**, 231–238, 1978.

Hilgers, A., B. Holback, G. Holmgren, and R. Boström, Probe measurements of low plasma densities with applications to the auroral acceleration region and auroral kilometric radiation sources, *J. Geophys. Res.*, **97**, 8631–8641, 1992.

Ishisaka, K., T. Okada, Y. Kasaba, K. Tsuruda, H. Matsumoto, H. Hayakawa, H. Kojima, and F. S. Mozer, Estimation of the electron temperature in the solar wind and electron foreshock by using GEOTAIL spacecraft potentials and plasma waves, *The transactions of the institute of electronics, information and communication engineers B* (Denshi Joho Tsushin Gakkai Ronbunshi), **J82-B**, 1239–1246, 1999 (in Japanese).

Matsui, H., T. Mukai, S. Ohtani, K. Hayashi, R. C. Elphic, M. F. Thomsen, and H. Matsumoto, Cold dense plasma in the outer magnetosphere, *J. Geophys. Res.*, **104**, 25077–25095, 1999.

Mott-Smith, H. M. and I. Langmuir, The theory of collectors in gaseous discharges, *Phys. Rev.*, **28**, 727–763, 1926.

Mozer, F. S., E. W. Hones, Jr., and J. Birn, Comparison of spherical double probe electric field measurements with plasma bulk flows in plasmas having densities less than 1 cm^{-1}, *Geophys. Res. Lett.*, **10**, 737–740, 1983.

Mukai, T., S. Machida, Y. Saito, M. Hirahara, T. Terasawa, N. Kaya, T. Obara, M. Ejiri, and A. Nishida, The low energy particle (LEP) experiment onboard the GEOTAIL satellite, *J. Geomag. Geoelectr.*, **46**, 669–692, 1994.

Nishida, A., The GEOTAIL mission, *Geophys. Res. Lett.*, **21**, 2871–2873, 1994.

Pedersen, A., Solar wind and magnetosphere plasma diagnostics by spacecraft electrostatic potential measurements, *Ann. Geophys.*, **13**, 118–129, 1995.

Pedersen, A., R. Grard, K. Knott, D. Jones, A. Confalone, and U. Fahleson, Measurements of quasi-static fields between 3 and 7 earth radii on GEOS-1, *Space Sci. Rev.*, **22**, 333–346, 1978.

Pedersen, A., C. A. Cattell, C.-G. Fälthammar, V. Formisano, P.-A. Lindqvist, F. Mozer, and R. Torbert, Quasistatic electric field measurements with spherical double probes on the GEOS and ISEE satellites, *Space Sci. Rev.*, **37**, 269–312, 1984.

Schmidt, R. and A. Pedersen, Long-term behaviour of photo-electron emission from the electric field double probe sensors on GEOS-2, *Planet. Space Sci.*, **35**, 61–70, 1987.

Tsuruda, K., H. Hayakawa, M. Nakamura, T. Okada, A. Matsuoka, F. S. Mozer, and R. Schmidt, Electric field measurements on the GEOTAIL satellite, *J. Geomag. Geoelectr.*, **46**, 693–711, 1994.

T. Nakagawa (e-mail: nakagawa@titan.tohtech.ac.jp), T. Ishii (e-mail: jl2ogz@mdn.gr.jp), K. Tsuruda (e-mail: tsuruda@stp.isas.ac.jp), H. Hayakawa (e-mail: hayakawa@stp.isas.ac.jp), and T. Mukai (e-mail: mukai@stp.isas.ac.jp)